LAND COVER MAPPING OF WETLAND AREAS IN AN AGRICULTURAL LANDSCAPE USING SAR AND LANDSAT IMAGERY

C. Castañeda[1], D. Ducrot[2]

[1]Soils and Irrigation Department, Agri-Research Center of Aragón, PO Box 727, 50080 Zaragoza, Spain

[2]Centre d'Études Spatiales de la Biosphère, CESBIO, 18 av. E. Belin, bpi 2801, 31401 Toulouse cedex 9, France.

Abstract

Saline wetlands in the Monegros Desert, NE Spain, are situated in an agricultural landscape which is undergoing significant changes. Agricultural intensification in recent decades and current installation of new irrigation systems threaten these valuable habitats, set to be included in the Natura2000 network. Their preservation and successful management depend on the information available regarding the transformation of surrounding areas. When soil and vegetation maps at adequate scale are not available, remote sensing is an alternative means to obtain needed data. We have used SAR data, taking advantage of the soil surface characteristics perceived in SAR images. The objective of this work is to explore the capability of multitemporal SAR data to characterize the land covers of these wetlands and their environment. We have developed specific contextual classifications which take into account the statistical properties of the radar distribution. Moreover, we tested the contribution of radar in Landsat classification.

Keywords: radar, fusion, classification, segmentation, arid, soil.

1. Introduction

Inland saline wetlands in dry environments are scarce in Europe and are not well represented in inventories and conservation plans. Due to growing recognition of their ecological significance, similar wetlands in other semiarid regions throughout the world have been inventoried and described (Dini et al., 1998). To this end, the U.S. Fish and Wildlife Service catalogues these wetlands as *Isolated Wetlands* of the *Playa* and *Salt Flat* types (Tiner et al., 2002). The U.S. Environmental Protection Agency (2005) has included *Playa-lake* in the classification system used in the National Wetlands Inventory (Cowardin et al, 1995).

The Monegros playa-lakes area, included in the Inventory of Geological Points since 1995, and unsuccessfully proposed for National Park status by conservationists decades ago, is officially recognized as meeting European standards for areas of ornithological value. A small number of the playa-lakes appear on the official topographic maps as marshes. They are not included in the Ramsar list.

Until now, no comprehensive map of these wetlands has been available, and their ecology has not been studied to establish criteria for their recognition. Due to the lack of soils and vegetation maps of the area, research efforts have centred on finding tools that can distinguish the wetlands —facies and influence area— from the surrounding land cover types by using remote sensing. This work concentrates on the discrimination of land covers in the wetlands area by means of radar data alone and coupled with Landsat images, adapting the treatment to the characteristics of the study area.

2. Areas of flooding and extreme salinity

A constellation of almost a hundred of saline wetlands —more than 1 000 ha of wetland area— are spread over an agricultural landscape of about 36 000 ha (Figure 1), in one of the most arid regions in Europe (Herrero and Snyder, 1997). Traditionally considered an agricultural wasteland or barren terrain from the point of view of productivity, in recent years the area has been besieged by agricultural intensification limited only by spots of flooding and extreme salinity. These saline wetlands play an important role in regional hydrology (Castañeda and Herrero, 2005). Furthermore, Monegros wetlands provide habitats recognized in the EU Natura2000 network (Domínguez et al., 2006) and host endemic species and other elements of biomass not yet protected by legislation, such as algae and extremophile microbes.

Figure 1

The wetlands area appears as a uniform dry farming area in the Corine LandCover 2000 map. However, these depressional and isolated wetlands (Leibowitz and Nadeau, 2003) usually stand out in the landscape (Figure 2) due to their flat bed topography with water and/or salt efflorescence, permanently wet soil related to their groundwater discharge function, and specific (halophilous) vegetation. There is a lack of soil and vegetation maps of the area that permit the identification of the saladas and their area of influence and that can be used to monitor the environmental changes caused by agricultural intensification and the installation of new irrigated areas. In one hand, land consolidation and intensive plowing have destroyed most of the native vegetation and have changed the shape of the fields. In the other hand, irrigation will modify the flooding period of these wetlands destroying the current geomorphological

dynamic. This result can be observed in other Spanish saline wetlands which experience permanent flooding and inflows of fresher water (Herrero and Castañeda, *in revision*).

Figure 2

3. SAR radar images for soil surface recognition

Remote sensing based on radar imagery is useful to obtain ground surface information on wetlands (Ozesmi and Bauer, 2002). Given that a large part of the study area is a horizontal platform, SAR imagery has been considered of interest because of its capacity to detect surface features related with wetness and roughness, two interesting parameters for depicting this area.

We employed a data-set of 3 SAR images during the cereal growing season to one year period taking into account that this number of images produce correct results though 5 dates are advisable to increase the accuracy with multitemporal SAR classifications (Ducrot et al., 1998). We selected three PRI SAR ERS-2 images from 2002 covering the early spring (2 March), late spring (15 June) and summer (24 August) —the period experiencing the greatest changes. Previous knowledge about these wetlands —soil surface changes, hydrological regime and agricultural practices— were essential since there was no available ground truth simultaneous to the ERS-2 passes. The annual ploughing allowed under the Common Agricultural Policies (CAP) leads to frequent and unpredictable changes in the surface of the fields with subsequent changes in roughness. Visualization of Landsat images belonging to the same seasons helped to understand the variation of the radiometry of the ERS images.

4. Multitemporal SAR data set

4.1. Images pretreatment

The use of radar datasets is common when differentiating surfaces in radar images under the speckle interference (Chust et al., 2004). Before image co-registration, we performed a visual analysis of each single-date image; the rainfall and wind registers simultaneous to the image acquisitions were examined in order to detect possible effects on the radar signal. March and June images were co-registered to the August image using 40-50 ground control points and a second degree polynomial function. Although cubic convolution is considered an adequate resampling method for preserving the structures and the linear features in radar images, we applied the nearest neighbour method to maintain, as much as possible, the original radiometry before filtering (Rataboul, 2001). The pixel size was 12.5 m, corresponding approximately to a surface area reflectivity of 25 m of side.

Segmentation of the multitemporal image was applied for both filtering and contextual classification. We used the ROEWA operator (Ratio of Exponentially Weighted Average) —the adapted version of the Shen and Castan operator (Fjørtoft et al., 1997) for optical imagery— since it takes into account the speckle of radar images. After applying different levels of contours, we selected the most suitable edge strength map according to the size of the wetlands and the natural and farming features in the area. We applied the watershed algorithm (Fjørtoft et al., 1997) on the edge strength map in order to obtain an image of closed skeleton contours. Next, a labelled region image (Fig. 3), i.e., a map of homogeneous regions, was created. For the classification,

113 we choose a relatively detailed segmentation, which in an agricultural area facilitates
114 correct classification.

115 Figure 3

116 The speckle inherent in radar images necessitates the use of filtering processes
117 prior to other treatments although this has the disadvantage of the loss of image
118 information, especially the structures and linear features. The multitemporal SAR image
119 was filtered by means of the adaptive filter LVMMSES (Linear Vectorial Minimum
120 Mean Square Error filter based on Segmentation) (Fjørtoft et al., 1997). This filter is
121 multitemporal, i.e. a series of radar images is required, and is based on the minimization
122 of mean square error between the estimation of radiometric value of the pixel and the
123 real value. The statistics are calculated on the regions defined by image segmentation.
124 The main advantage of the LVMMSES filter is that it preserves the contours and linear
125 structures of the image.

126 *4.2. Classification process*

127 The segmentation was also introduced in the classification process of the
128 multitemporal ERS-2 image. The classifications performed were based on contextual
129 methods, e.g., taking into account the neighbourhood of each pixel inside a sliding
130 window or a region defined by image segmentation. The non supervised ―automatic―
131 method was applied to explore the characteristics of the image before using supervised
132 method. Since there was no ground truth simultaneous to the ERS passes, interpretation
133 of Landsat images belonging to the same seasons was used as a reference for the
134 training process.

135 The training areas were collected over the SAR RGB multitemporal
136 composition. The classes established were adapted to the photo-interpretation of the
137 optical images and the physical interpretation of the radar signal. In this way, a
138 combined and interactive image analysis (Figure 4) was carried out based on previous
139 knowledge of the study area.

140 Figure 4

141 The following five general covers were sampled: *irrigated land*, *non-irrigated*
142 *land, natural vegetation*, *wetlands,* and *river*. Moreover, two specific radar classes were
143 sampled: *high reflectors* and *radar shadow*, both of which are related to the geometry
144 perceived by radar images. Because of the great amount of information from radar
145 images —making their reading complex— each precedent class showed variable
146 backscattering in the radar RGB combination. In order to get the best possible
147 information from each data source —optical and radar—, it was necessary to establish
148 subclasses within each previous class. A total of 27 different classes were sampled and
149 statistically analysed to detect heterogeneity in their distribution; we could observe also
150 the *a priori* separability of the classes, the contribution of each channel, and the channel
151 where each class was best discriminated.

152 The training areas were created automatically from the segmented image to
153 guarantee a more accurate and statistically homogeneous temporal sampling. Two
154 groups of training samples were created, for classification and verification, respectively.
155 We applied two classification methods: (i) the ICM method (Iterative Conditional
156 Mode) (Besag, 1974), based on a Markov region model, was executed in non supervised
157 and supervised modes; and (ii) the CMLGW method (Contextual Maximum Likelihood

158 based on the Gauss-Wishart law) (Chust et al., 2004). Different parameters —the
159 number of iterations and classes, the window size and the textural information— were
160 tested in order to achieve the maximum discrimination inside the wetlands and the
161 minimum confusion outside them. Moreover, we built three new channels
162 corresponding to the three coefficients of variation C —σ/μ—, of each radar image
163 calculated on a neighbourhood of 3×3 pixels. We introduced these new channels in the
164 classification process. Finally, post-classification improvements were performed.

165 Statistical and visual criteria were used to assess the classification accuracy. The
166 statistical criteria were based on the confusion matrix created from the comparison
167 between the classification and the verification data. Generated from this confusion
168 matrix, the percentage of Pixels Correctly Classified (PCC) and the kappa coefficient of
169 agreement (κ) (Congalton, 1991) were analysed to assess the discrimination of classes.
170 The visual criteria were useful when taking decisions about regrouping the subclasses.

171 *4.3. Fusion of radar and optical data*

172 We exploited the potential of radar to improve the classification of optical
173 images. A set of 18 multispectral channels corresponding to the 1-5 and 7 bands of the
174 three Landsat ETM+ images acquired in March, June and August 2000 was employed.
175 We applied two fusion approaches: (i) the Bayesian method, by concatenation of ERS
176 channels to the Landsat ETM+ bands, and (ii) the fusion of classifications based on the
177 possibility and evidence theory (Shafer, 1976). This last method modelled the ignorance
178 and missing information and measured the degree of conflict between the two sources.
179 Previously, Landsat and SAR imagery were georeferenced and resampled to 25 m of
180 pixel size, and separately classified. Intersection of classes from the two sources was

181 measured using the confusion matrix: the concordance was enhanced and the conflicts
182 attenuated (Chust et al., 2004).

183

184 **5. Results**

185 *5.1. Understanding the scene variables*

186 Physical interpretation of radar reflectivity levels in this area was difficult even
187 in multitemporal compositions because of the uncertainty included in the backscattering
188 information. Though the unfiltered multitemporal image supplied more information
189 than the filtered image, the latter was preferred to perform visual analysis and to take
190 ground control points during georeferencing process.

191 In spite of rain registered simultaneously to the satellite pass in March and
192 August, the area did not show evidence of freshly moistened soil surfaces. The largest
193 wetlands were visually discriminated on each date because their wet and flat bottom
194 produced in general a mirror response; the grey tone levels in the bottom can be
195 interpreted as roughness produced by desiccation polygons, algal mats, efflorescence, or
196 water rippled by the wind. This uncertainly makes the systematic discrimination of the
197 wetland facies (Castañeda et al., 2005) difficult; many structural features appear, some
198 of them created by the speckle contribution.

199 Wetlands appear in the multitemporal RGB combination with different coloured
200 areas. Because of the lack of simultaneous ground data and the variety of causes
201 involved, it was not possible to assign them a thematic meaning. Thus, they were
202 described on the basis of roughness variation. The water body was not systematically

discriminated by means of visual interpretation because the corresponding backscatter could vary depending on the wind: from low values similar to those of the flat bottom up to high values similar to those of rainfed fields.

The RGB composition enhances changes in radiometry in the fields. Simultaneous details about the agricultural practices would have been necessary to interpret this variability, especially in the rainfed area, where variability in radiometry was interpreted as differences in roughness more than in wetness.

5.2. SAR classification

From non supervised classification we observed that the irrigated crops, the river, and the largest wetlands were clearly but not perfectly detached from the background. General noise was observed and wetland bottoms were confused with the river. These results were used as a guide for sampling the training areas in the supervised classification.

The ICM method yielded the lowest statistical results, slightly increased using context information in a 3×3-window size. The CMLGW method improved the discrimination of the classes, both visually and statistically, though general noise remained. Table 1 show the statistical values obtained from different multitemporal classifications. From the three coefficients of variation extracted from the original SAR images, only that of the August channel (C_3) enhanced the classification. A 3×3 window size kept the information inside the wetlands, while the 7×7 window size was useful to remove the noise outside them. We applied the fusion of the best classifications obtained with the CMLGW method using a 3×3 window size for context information.

225 The contribution of C_3 and the post-classification processes resulted in slightly
226 increased PCC and κ, 65.5 and 59.7, respectively.

227 The largest wet, flat wetlands were identified (Figure 5), together with a part of
228 their halophytic fringes; the smallest wetlands, those covered by halophytes and smooth
229 borders were lost. In general, the wetland borders were blurred due to the speckle; only
230 some of them were partially outlined by the *radar shadow* produced by their talus.

231 Figure 5

232 Outside the wetlands, the classification discriminated the irrigated areas, the
233 river, and geomorphologic features related to the relief. Two regions are clearly
234 differentiated in the dry farming area surrounding the wetlands (Figure 6).

235 Since there are no significant differences in slope or geometry, the soils are
236 poorly differentiated —shallow *A* horizon with very low content in organic matter—
237 and the vegetation is sparse, segregation was related to differences in the dielectric
238 response of the terrain —lithology/soil—. Regarding the geology, the two different
239 regions correspond to: (i) a lutite and gypsum-rich area in the northern part of the
240 image, and (ii) a limestone area in the southern part. This lithological information was
241 kept in the final legend since it encompassed subclasses with different radiometry.

242 Figure 6

243 When the 27 total classes were grouped in 11 thematic classes, the PCC and κ
244 increased to 75.2 and 64.8, respectively. However, visual analyses showed the missing
245 details, especially inside the wetlands. The class *high reflectors* increased the confusion
246 in relief areas, and linear structures such as the river and roads were lost. We have

obtained a first approach to creating a land cover map of the Monegros wetland area through a multitemporal approach based on 3 dates.

5.3. SAR and Landsat data fusion

The classification of the geo-referenced SAR images provides misleading information due to the addition of image treatments. Details inside the wetlands and the linear structures, such as river and roads, were lost, even with a small window used for the contextual information.

The Landsat multitemporal classification provided the best results when using the 18 multispectral bands, with PCC and κ equal to 81.1 and 69.2, respectively. The river, the wetland contour and the vegetation were better discriminated, and crops at different stages of development were noticeable. In spite of this, the borders of the fields and the relief did not appear. The radar contribution in the multisensor classification was clear, since the resulting classified image preserved the visual aspect of radar images in spite of the high number of optical channels used. Compared with the SAR-alone classification, the multisensor image formed by 21 channels —18 from Landsat and three from ERS— improved PCC and κ values to 89.2 and 88.0, respectively. Results of the fusion of Landsat and radar classifications (Figure 7) offer slightly higher accuracy with PCC and κ equal to 86.5 and 84.0, respectively. The fusion of Landsat and SAR data improved the classification of each data-set separately. The boundaries of the fields and radiometric differences were enhanced; the natural vegetation presented less confusion.

Table 1

Figure 7

The structure of the landscape —linear features, soil surface roughness, and the relief areas— was preserved by improving the discrimination of the classes associated with the relief. The edges of the fields, both irrigated and rainfed, were enhanced. Discrimination of natural vegetation in the bordering relief areas increased, although the xerophytes of plain areas appeared undifferentiated from non-irrigated crops. Distinction of wetlands was enhanced since bottoms stand out from the surroundings by their clear borders. The discrimination of the wetlands facies was not significantly improved. The two specific radar classes disappeared almost completely.

A sound thematic map of the area is achieved. For environmental monitoring purposes, a field campaign simultaneous to the images is desirable to identify the surface aspects involved in the variability of the radar classes. This map, representing a moment of time, can be repeated in a number of years after in order to detect the agricultural changes related with the advance of irrigation. Moreover, taking advantage of the historical archive of ERS-1 and ERS-2 imagery, a retrospective map can be done in order to find long-term changes in the wetland surroundings.

6. Conclusions

We have extracted multitemporal radar information from SAR imagery of the Monegros saline wetlands and their surroundings. The segmentation and filtering of the SAR images was adapted to preserve both radiometry and structures. The images

292 treatment was tailored to the singular characteristics of the wetland area and to the lack
293 of simultaneous *in situ* data.

294 Multitemporal contextual classification of three selected dates —chosen
295 according to the culture calendar— have discriminated the main land covers of the area,
296 although to obtain the most satisfactory results. In spite of the uniformity of the flat
297 bottoms these wetlands were classified in heterogeneous regions related to the
298 roughness perceived by the C band of the ERS sensor.

299 The fusion of Landsat and ERS data leads to better class separability. The
300 benefit of Landsat channels for discriminating type of vegetation —irrigated crops and
301 xerophytes— was complemented by the perception of the structure of the landscape: the
302 discrimination of the classes associated with the relief was improved, and the wetland
303 bottoms were enhanced and outlined.

304

305 **Acknowledgements**

306 This work was carried out as part of projects REN2003-00742 and AGL2006-
307 01283, both granted by the Spanish Ministry of Education and Science an FEDER. A.
308 Lopès provided helpful comments on radar signal interpretation.

309

310 **References**

311 Besag, J., 1974. Spatial interaction and the statistical analysis of lattice systems (with
312 discussions). Journal of the Royal Statistical Society 36, 192-236.

313 Castañeda, C., Herrero, J., 2005. The water regime of the Monegros playa-lakes
314 established from ground and satellite data. Journal of Hydrology 310, 95-110.

315 Castañeda, C, Herrero, J., Casterad, M.A., 2005. Facies identification within the playa-
316 lakes of the Monegros Desert, Spain, with field and satellite data. Catena 63, 39-
317 63.

318 Chust, G., Ducrot, D., Pretus, J.L., 2004. Land cover discrimination potential of radar
319 multitemporal series and optical multispectral images in a Mediterranean cultural
320 landscape. International Journal of Remote Sensing 5 (17), 3513-3528.

321 Congalton R.G., 1991. A review of assessing the accuracy classification of remotely
322 sensed data. Remote Sensing of Environment 37, 35-46.

323 Cowardin, L.M., Golet, F.C., 1995. US Fish & Wildlife Service 1979 wetland
324 classification: a review. Vegetatio 118, 139-152.

325 Dini, J., Cowan G., Goodman P., 1998. South African National Wetland Inventory.
326 Proposed wetland classification system for South Africa. Available on:
327 www.environment.gov.za-/soer/nsoer/resource/wetland/index.htm.

328 Domínguez, M., Conesa, J.M., Pedrol, J., Castañeda, C., 2006. Una base de datos
329 georreferenciados de la vegetación asociada a las saladas de Monearos. In:
330 Camacho, M.T., Cañete, J.A., Lara, J.J. (Eds.), El acceso a la información espacial
331 y las nuevas tecnologías geográficas, Proc. XII Congreso Nacional de Tecnologías
332 de la Información Geográfica, Granada, Spain.

333 Ducrot, D., Sassier, H., Mombo, J., Goze,S. Planes, J.G., 1998. Contextual methods for
334 multisource land cover classification with application to Radarsat and SPOT data.
335 Proc. SPIE 3500, 225.

336 Fjørtoft, F. Séry, D. Ducrot, A. Lopès, C. Lemaréchal, C. Fortier, P. Marthon, E.
337 Cubero-Castan, 1997. Segmentation, Filtering and Classification of SAR Images.
338 Proc. VIII Latin American Symposium on Remote Sensing (SELPER'97), Mérida,
339 Venezuela.

340 Herrero, J., Snyder, R.L., 1997. Aridity and irrigation in Aragón, Spain. Journal of Arid
341 Environments 35, 55-547.

342 Herrero, J., Castañeda, C. Delineation and functional status monitoring in small saline
343 wetlands of NE Spain. Catena, *in revision*.

344 Leibowitz, S.G., Nadeau, T.L., 2003. Isolated wetlands: state-of-the-science and future
345 directions. Wetlands 23, 663-684.

346 Ozesmi, S.L., Bauer, M.E., 2002. Satellite remote sensing of wetlands. Wetlands
347 Ecology and Management 10, 381-402.

348 Rataboul, X., 2001. Élaboration d'un protocole de classification et fusion d'images
349 radar et optiques. CESBIO, Toulouse.

350 Shafer, G., 1976. A mathematical theory of evidence, Princeton University Press.

351 Tiner, R.W., Bergquist, H.C., DeAlessio, G.P., Starr, M.J., 2002. Geographically
352 Isolated Wetlands: a preliminary assessment of their characteristics and status in
353 selected areas of the US. U.S. F&W Service, MA.

354

355 **List of Figures**

356

369

370 **Tables**

371

372 Table 1

373 The percentage of Pixels Correctly Classified (PCC) and the kappa coefficient of

374 agreement (κ) obtained from the different multitemporal classifications.

375

Multitemporal classifications	PCC	κ
SAR + coeficient of variation	65.5	59.7
SAR + coeficient of variation	75.2	64.8
Landsat	81.1	69.2
SAR + Landsat :Multisensor classification	89.2	88.0
SAR + Landsat :Fusion of classificactions	86.5	84.0

376

377

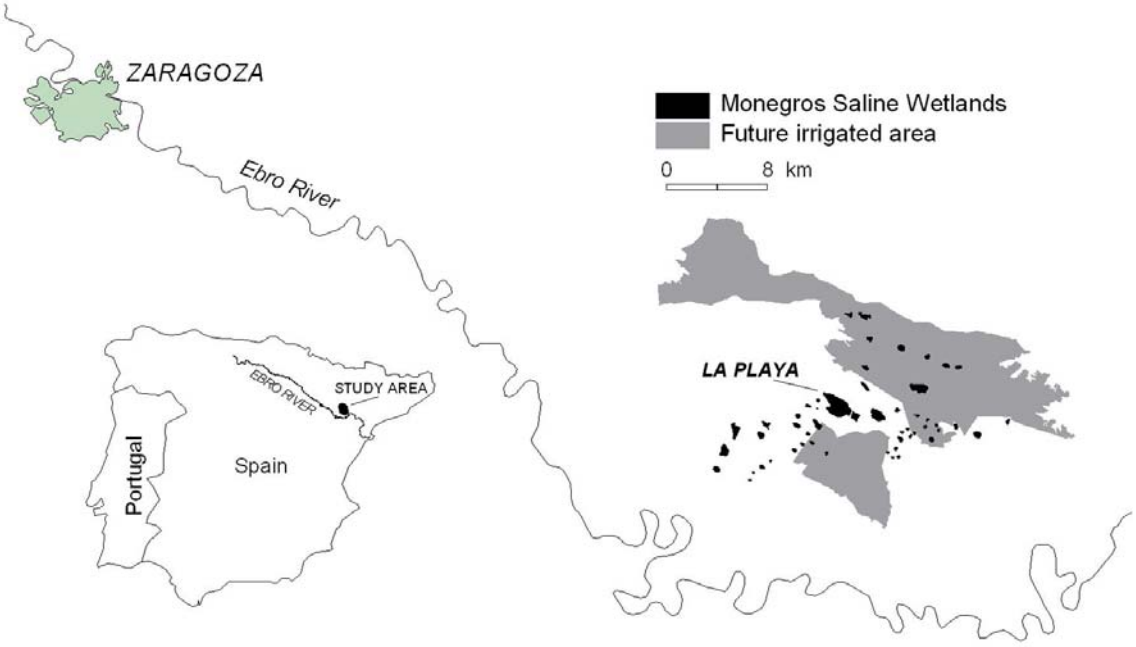
ZARAGOZA
Ebro River
Monegros Saline Wetlands
Future irrigated area
0
8 km
LA PLAYA
EBRO RIVER
STUDY AREA
Portugal
Spain

378

379

380

381

382 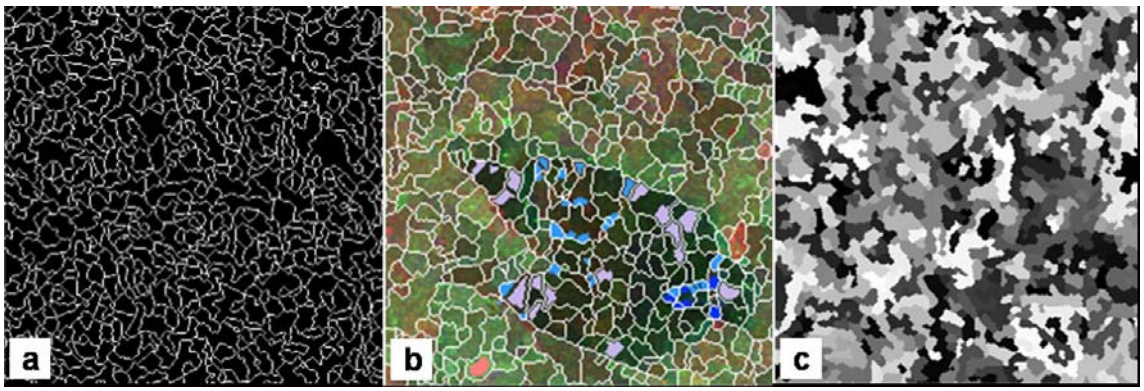

383

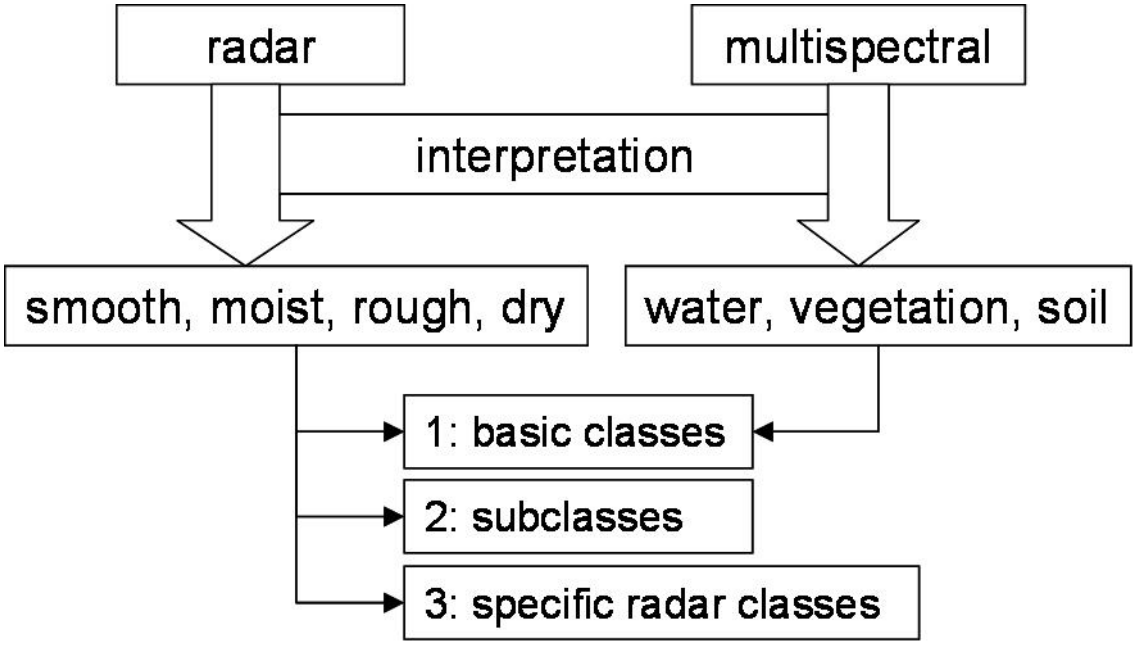
radar
multispectral
interpretation
smooth, moist, rough, dry
water, vegetation, soil
1: basic classes
2: subclasses
3: specific radar classes

384

385

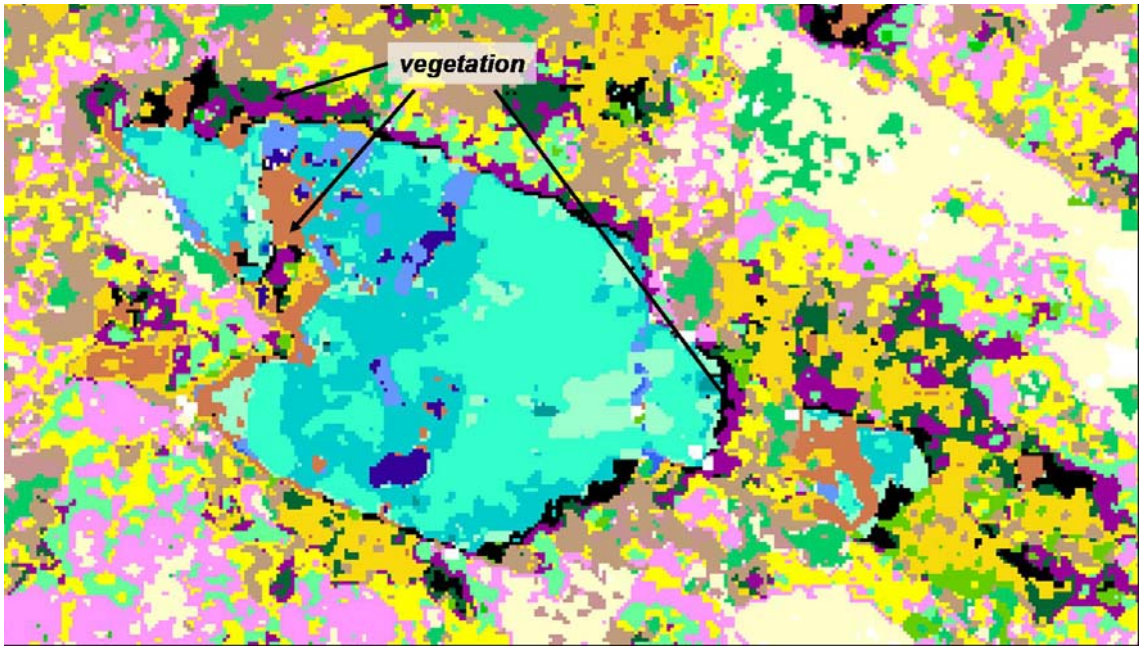

386

387

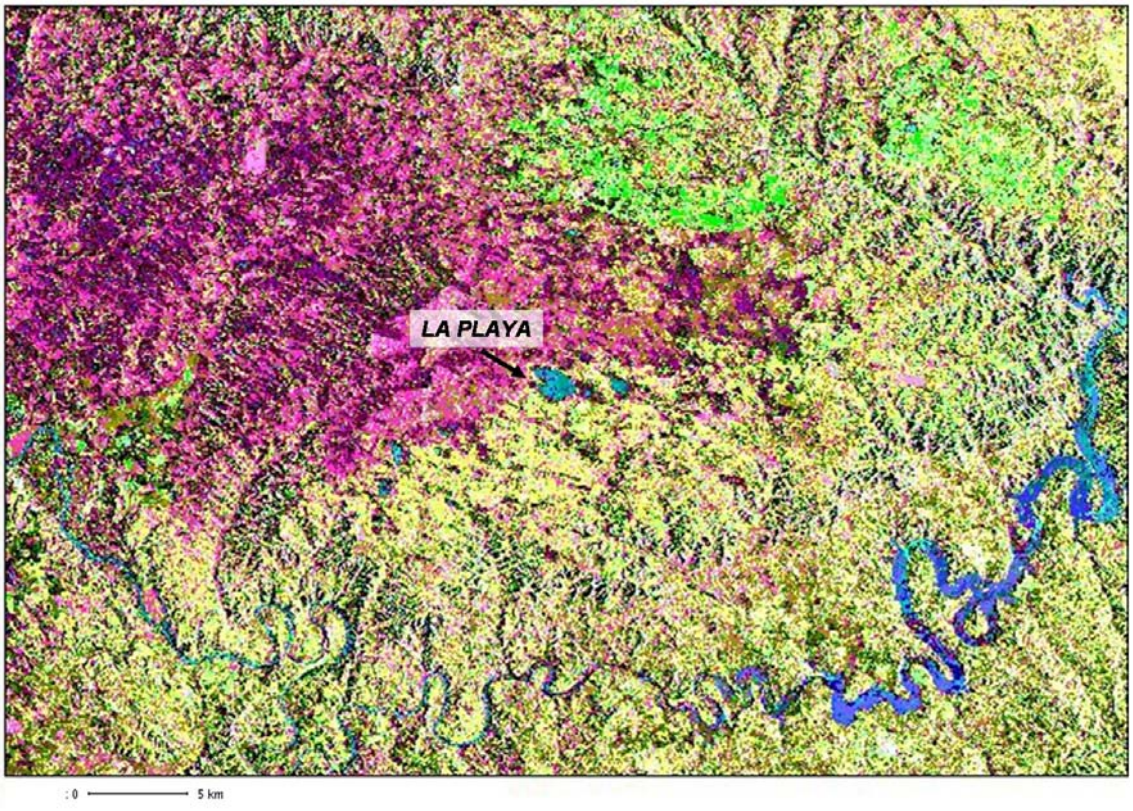

388

389

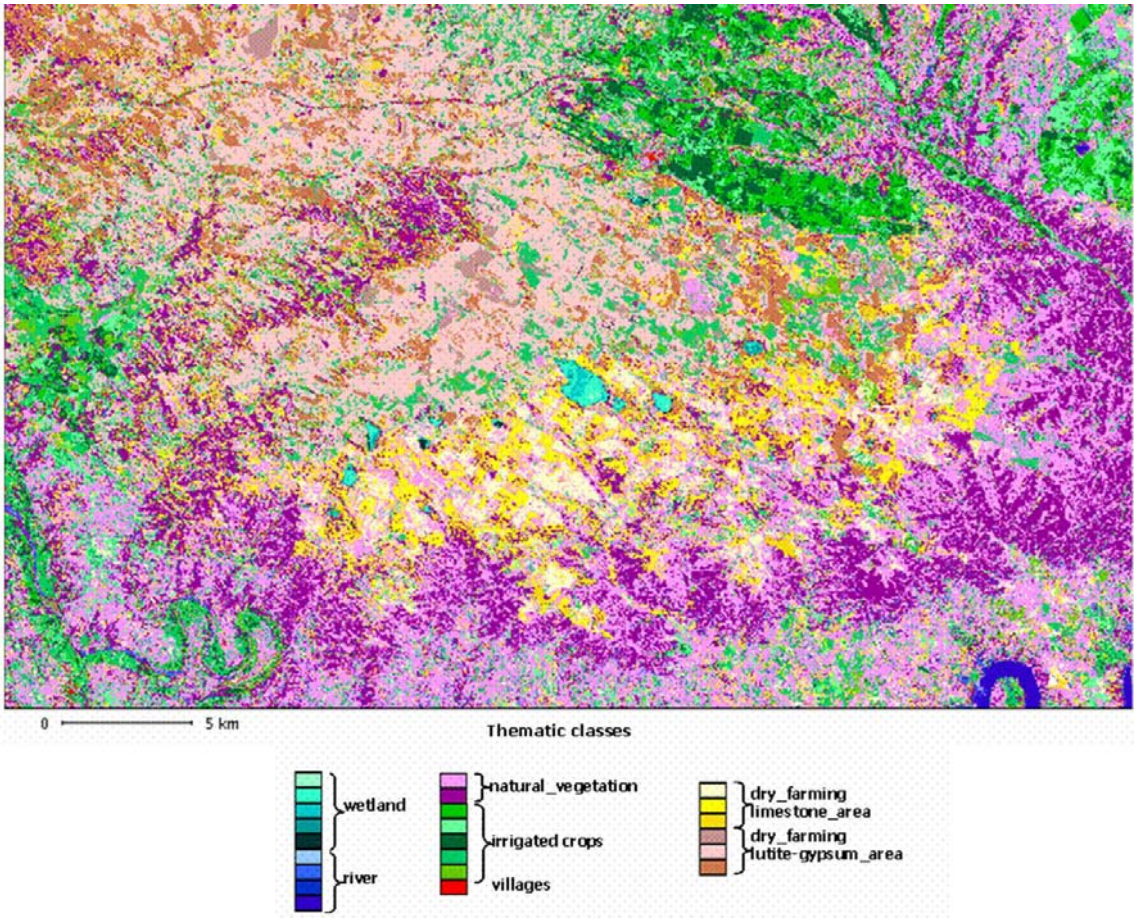
0
5 km
Thematic classes
wetland
river
natural_vegetation
irrigated crops
villages
dry_farming
limestone_area
dry_farming
lutite-gypsum_area

390

391

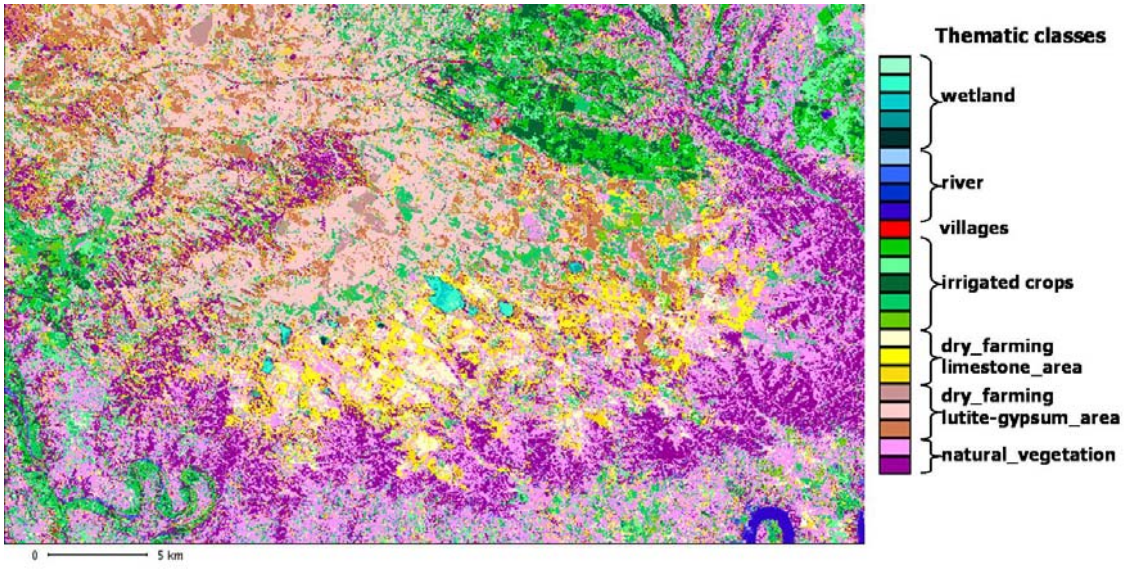
Thematic classes
wetland
river
villages
irrigated crops
dry_farming
limestone_area
dry_farming
lutite-gypsum_area
natural_vegetation
0
5 km

392